DNA condensation-inspired assembly of DNA nanotubes into reversible superstructures: the value of valency

Laura Bourdon,[1] Xiang Zhen Xu,[2] Mathieu Morel,[1] Sergii Rudiuk,[1] Ayako Yamada,[1] Damien Baigl[1]*

[1]PASTEUR, Department of Chemistry, École Normale Supérieure, PSL University, Sorbonne Université, CNRS, 75005 Paris, France

[2]Laboratoire de Physique et d'Etude des Matériaux (LPEM), CNRS UMR 8213, ESPCI-Paris, PSL Research University, Sorbonne Université, 10 rue Vauquelin, Paris, 75005 France

*correspondence to: damien.baigl@ens.psl.eu

Abstract

We report that self-assembled DNA nanotubes, upon the addition of DNA condensing multivalent cations, including the naturally occurring polyamines spermidine and spermine, spontaneously condense to form higher-order structures including micrometer-sized rings, vast tridimensional networks and highly clustered bundles. We demonstrate that the process is electrostatically driven, conferring a ubiquitous character to this assembly principle, with a pivotal role of the counter-ion valency. This allows us to devise methods for additional control, such as superstructure disassembly upon monovalent ion addition or photocontrol using a photosensitive DNA condensing agent.

Introduction

Structural DNA nanotechnology has emerged as a versatile tool to build elaborate nanostructures in a convenient, biocompatible and user-friendly way.[1] By exploiting specific DNA base-pairing principles, it is now possible to program the assembly of cocktails of synthetic DNA strands into virtually any desired 2D[2,3] or 3D[4–6] morphologies. The resulting structures are not only obtained at a high yield with great precision, but they can also be used as universal scaffolds to spatially organize bound entities (proteins, particles, etc.) with subnanometric resolution, leading to a vast range of applications, from materials science to biomedicine.[7,8] The underlying DNA self-assembly principles impose however some limits. First, most approaches rely on the use of a scaffold, as in the case of DNA origamis,[2] which strongly limits the size of the final self-assembled structures, typically up to around 100 nm, unless specific additional protocols are applied.[9,10] Additionally, despite the recent development of isothermal DNA self-assembly principles,[11] the vast majority of methods rely on a thermal annealing step to ensure flawless assembly between the multitude of DNA strands.[12] This temperature treatment, consisting in heating the system above the melting temperature before a slow cooling down ramp, takes usually hours to days, thus imposing strong temporal constraints on the assembly. To expand the potential offered by programmable DNA self-assembly, it would be highly valuable to identify principles orthogonal to base-pairing rules, in which DNA nanostructures could be assembled into well-defined superstructures, both extended in space and produced in a rapid manner. We suggest to approach such a goal by getting inspired by the fact that, in nature, DNA is usually present in a variety of higher-ordered structures not solely relying on Watson-Crick-Franklin interactions. For instance, genomic DNA of viruses, eukaryotes and prokaryotes are highly organized thanks to a combination of interactions where electrostatics plays a major role. It has been shown in particular that double-stranded DNA, which adopts an elongated coil conformation in water due to the strong electrostatic repulsions between the phosphate groups along its backbone, undergoes a dramatic transition into highly ordered structures, such as toroids, when small multivalent cations, including naturally occurring polyamines such as spermidine and spermine, are added.[13–15]

We envisaged that this principle could be used to rapidly reorganize self-assembled DNA nanostructures into higher-order superstructures. The exploitation of electrostatic interactions for such a purpose has already been explored but only in a few notable cases. In the case of DNA origamis, solid substrates were used to generate electrostatically tunable lattices[16–18] or induce intramolecular suprafolding transition in the case of soft cationic polymer layer.[19] The requirement of solid substrates limits however the versatility and applicability of the resulting assemblies. In bulk, intramolecular reconfiguration upon addition of positively charged proteins[20] and intermolecular assemblies mediated by cationic nanoparticles[21] were reported. However, DNA origamis, remaining small building blocks, are not well suited for the construction of extended 3D assemblies. For their elongated geometry and possibility to reach micrometric dimensions, DNA nanotubes obtained by the self-assembly of single-stranded or

double-crossover tiles, appear as more promising starting materials.[22–24] For instance, the addition of crowding agents or magnesium ions induced the formation of asters[25] or bundles,[26–28] respectively, while specifically designed macromolecular star-shaped cationic crosslinking agents led to contractile rings.[29] Surprisingly, the use of naturally occurring polyamines for the assembly of DNA nanotubes has never been explored. Moreover, although DNA condensation is a reversible process, the possibility of dynamically disassembling DNA nanotubes superstructures has been overlooked. Here, we used a simple cocktail of 5 DNA strands leading to long self-assembled nanotubes[22] and studied how they reorganized upon addition of two naturally occurring polyamines known as DNA condensing agents, the triamine spermidine (noted SPD^{3+}) and the tetraamine spermine (noted SPM^{4+}), and compared with the effect of magnesium ion (Mg^{2+}). Using fluorescence and electron microscopy, we revealed the reproducible formation of a diversity of superstructures, including bundles, rings as well as novel organizations into extended networks. We established phase diagrams highlighting the importance of counter-ion valency rather than specific interactions and proposed methods to reversibly disassemble the superstructures into nanotubes through monovalent salt addition. We also explored the possibility of photocontrolling the superstructure formation in the presence of a photosensitive DNA condensing agent.

Results and discussion

We used DNA nanotubes obtained by the thermal annealing of 5 short DNA strands (500 nM each, including a fluorescently labelled one) in a so called TAMg buffer (Trizma base 40 mM, acetic acid 20 mM, $MgCl_2$ 12.5 mM). We hypothesized that the addition of multivalent cations capable of DNA condensation would induce the formation of superstructures that could be disassembled with a further addition of monovalent ions in a sufficiently large excess (**Fig. 1A**). Initial nanotubes appeared as elongated filaments freely fluctuating in solution as observed by fluorescence microscopy (**Fig. 1B** *left*, *top image* and **Movie S1**). Transmission electron microscopy (TEM) revealed that they were well individualized (**Fig. 1B** *left*, *bottom image*) with a uniform diameter of 12 ± 3 nm (**Fig. S1A**), in agreement with previous reports.[22] We first added spermine (noted SPM^{4+}), a natural tetraamine, and observed the resulting structures in bulk by fluorescence microscopy. Addition of millimolar amounts of SPM^{4+} led to immediate formation of arrested structures of large dimensions floating in solution, with a low fluorescence background indicating that most nanotubes were engaged in these clustered structures (**Fig. 1B** *right*, *top image* and **Movie S1**). Similar assemblies were observed in the past using high concentrations of Mg^{2+} or crowding agents[26,28,29] and will be referred to as "bundles". Moreover, TEM revealed a local organization into thick elongated structures (**Fig. 1B** *right*, *bottom image*) with an average diameter of 63 ± 26 nm (**Fig. S1B**) where individual nanotubes could not be distinguished anymore, indicating a very strong attraction mediated by SPM^{4+}.

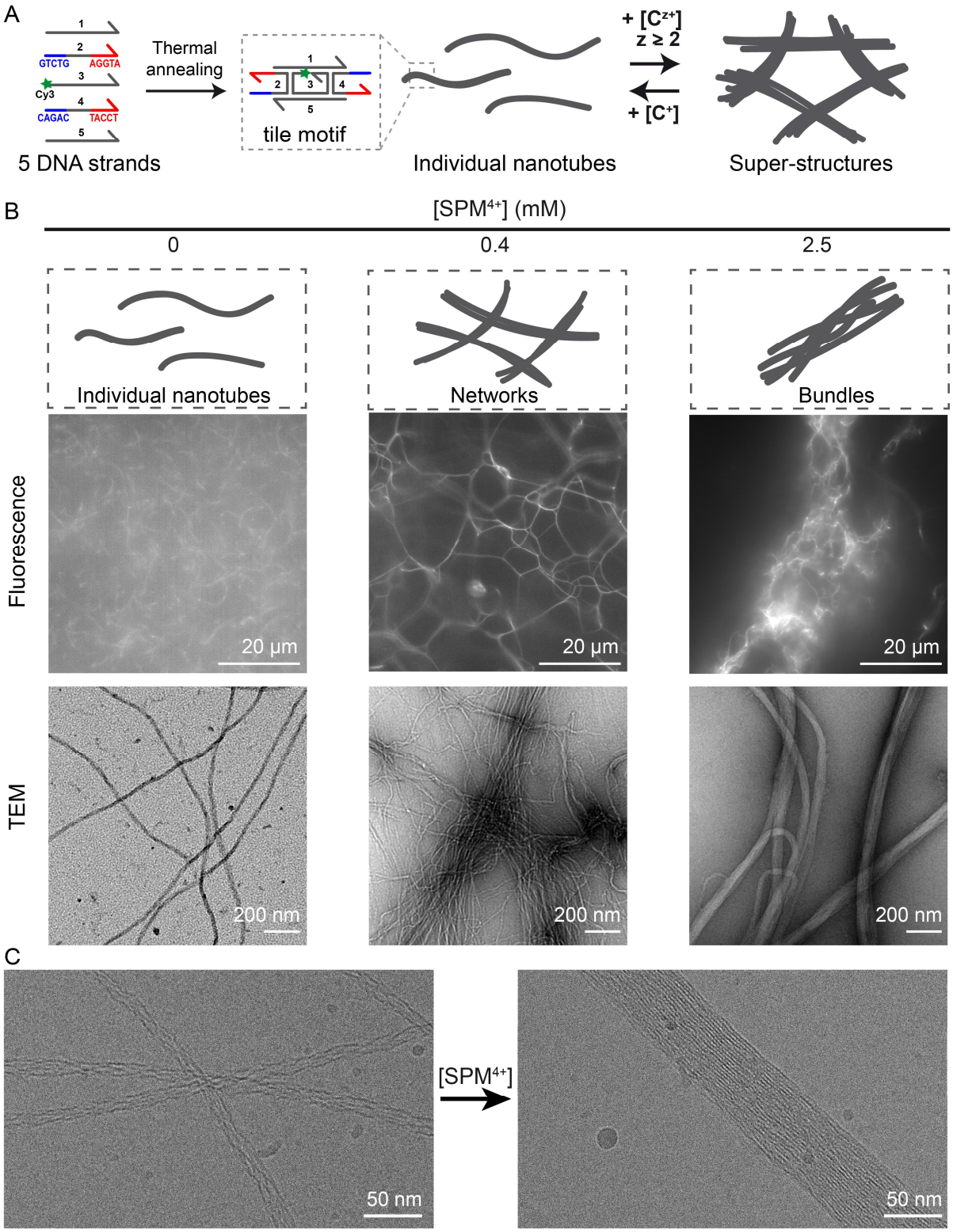

Figure 1. Multivalent cationic DNA condensing agents induce the assembly of individual DNA nanotubes into various superstructures. *A) Concept and experimental principle: individual nanotubes, prepared by thermal assembly of five DNA strands forming a self-associating tile motif, assemble into superstructures upon addition of multivalent cations (of valency z) that can be reversibly dissociated with an excess of monovalent cations. The central strand of the motif is labelled*

with Cy3 dye at its 5' end. B) Characterization of individual nanotubes and superstructures obtained with 0, 0.4 mM and 2.5 mM of spermine (SPM^{4+}), by epifluorescence microscopy (Cy3 fluorescence, top) and transmission electron microscopy (TEM, bottom). C) Cryo-electron microscopy of nanotubes before (left) and after (right) addition of 2.5 mM of spermine. Each DNA strand concentration is 500 nM in TAMg buffer.

Notably, for intermediate SPM^{4+} concentration, we observed an original interconnected organization (**Fig. 1B** *middle*). It consisted in highly fluorescent filaments connected into vast tridimensional networks with a mesh size varying within the range 5 – 20 µm (**Fig. 1B** *middle*, *top image* and **Movie S1**). Contrary to finite-size bundles, these interconnected structures occupied most of the solution. Interestingly, TEM revealed that individual nanotubes could be distinguished and were found to locally organized into aligned assemblies (**Fig. 1B** *middle*, *bottom image*), showing inter-tube attraction, but without strongly condensing as in the bundles.

It is known that electrostatic condensation of a semi-flexible polyelectrolyte like double-stranded DNA (dsDNA) leads to the formation of toroids with a diameter (≈ 100 nm) around twice its persistence length (50 nm),[15] inside which dsDNA double-helices are parallelly packed in a nearly crystalline manner with an interspacing of about 2.4 nm.[30] We thus scrutinized in more detail the regime of bundle formation ($[SPM^{4+}]$ = 2.5 mM). First, we used cryo-electron microscopy (cryo-EM) to reveal the internal structure of the DNA assemblies before and after bundle formation (**Fig. 1C**). Without SPM^{4+}, we could distinguish the DNA strands in the repeating tile motif forming hollow nanotubes with a diameter in agreement with TEM observations. Notably, after SPM^{4+} addition, hollow nanotubes could not be distinguished anymore. Instead, the inner structure of the bundles revealed a tightly packed parallel DNA arrangement with an interspacing of around 3 nm, *i.e.*, a value close to a double-helix diameter (2 nm). This feature, structurally reminiscent to the internal organization of condensed DNA in toroids, confirms the role of SPM^{4+} to induce electrostatic condensation of the nanotubes. Moreover, using TEM we detected that the condensed nanotubes also existed in the form self-closed structures similar to DNA toroids but of much larger dimensions (**Figs. 2A, 2B**). These rings were also observed by confocal microscopy coexisting with bundle fragments adsorbed on the microscopy cover slip surface (**Fig 2C** *left*, *white arrows*). Using super-resolution fluorescence imaging allowing a 120 nm lateral resolution, rings appeared with a single dense contour (**Fig. 2C** *right*), in agreement with cryo-EM (**Fig. 1C** *right*) and TEM (**Fig. 2B**) data, confirming the compact longitudinal assemblies of the nanotubes in these structures. The ring diameter was found to typically vary between 1 and 10 µm (**Fig. 2D**), with a mean ± SD value of 2.0 ± 1.7 µm (**Fig. 2E**), which is smaller yet of the order of twice the persistence length of nanotubes (≈ 4 µm) [22]. It is also in agreement with a recent report using a large synthetic star-shaped multicationic crosslinking agent.[29] Our results thus show that electrostatic DNA condensation by

counter-ion condensation is enough to generate the spontaneous formation of rings and, notably, does not require specific crosslinking interactions.

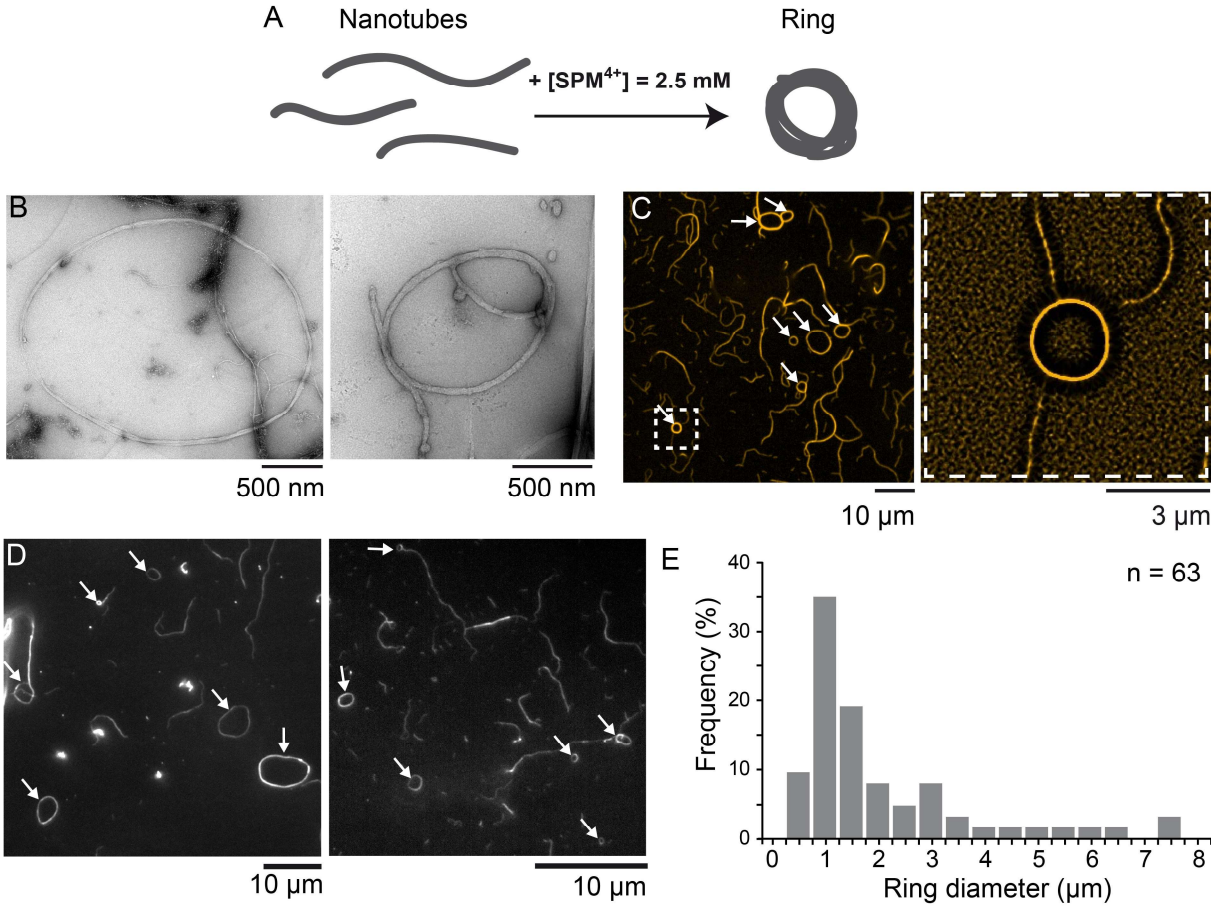

Figure 2. Sufficient spermine concentration (2.5 mM) induces the condensation of individual DNA nanotubes into ring-like structures. *A) Scheme of ring formation. B) Representative TEM images of the rings. C) Left, confocal images showing the rings adsorbed (indicated by white arrows) on the surface of a coverslip. Right, super-resolved image of the ring boxed by a dashed line on the left. D) Epifluorescence microscopy images of DNA rings adsorbed on a glass coverslip. E) Distribution of ring diameters established from epifluorescence imaging (n = 63). Each DNA strand concentration is 500 nM in TAMg buffer.*

To both understand the physico-chemical mechanisms underlying the formation of the different superstructures and analyse how general this behaviour could be, we established a diagram reporting the nature of the obtained superstructures for different multivalent cations added to DNA nanotubes. The diagram was plotted as function of both the condensing agent concentration (**Fig. S2**) and the charge ratio ρ (**Fig. 3**), which was defined as the concentration of charges brought by the condensing agent normalized by that of DNA (**Text S1**). Starting with spermine (SPM^{4+}), we observed the formation of networks from [SPM^{4+}] = 0.2 mM (ρ = 7.14) to 0.4 mM (ρ = 14.3) (**Fig. S3**). For larger concentrations, nanotubes were organized into bundles coexisting with a fraction of rings, in agreement with **Figs. 1–2**. Using spermidine (SPD^{3+}), a trivalent polyamine, a similar nanotube-network transition was observed

but at a higher concentration (5 mM, **Figs. S2, S4**). Interestingly, this concentration increase was larger than a simple compensation of valency as revealed by the larger charge ratio at the transition (ρ = 143, **Fig. 3**). We compared the effect of these two polyamines to the simple dication $Mg^{2+}$and found the same behaviour, at even a larger concentration (50 mM, **Figs. S2, S5**) and ρ (ρ = 1190, **Figs. 3**, **S5**), confirming not only the importance of valency in driving the process but also that such nanotube assembly mainly relies on electrostatic attraction rather than specific chemical interactions. For SPD^{3+}, bundles were observed for higher concentrations and charge ratios but were smaller in size that with SPM^{4+} while we could not detect bundles in the highest magnesium concentrations tested in our experiments. This further highlights the importance of a high condensation agent valency to get large and dense assemblies of DNA nanotubes.

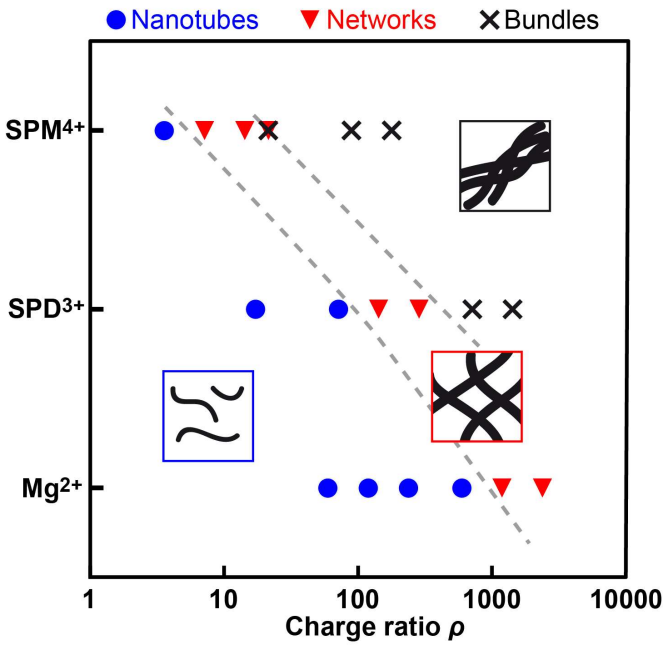

Figure 3. Nanotube assembly is electrostatically driven with efficiency strongly increasing with an increase in condensing agent valency. *Diagram showing the superstructures formed by the nanotubes after addition of different multivalent cations (magnesium Mg^{2+}, spermidine SPD^{3+} or spermine SPM^{4+}), as a function of the charge ratio ρ defined as the concentration of charges brought by the condensing agent normalized by that of DNA. Each DNA strand concentration is 500 nM in TAMg buffer.*

For a given valency, the evolution observed in all these phase diagrams is in agreement with the assembly of rigid negatively charged polyelectrolytes, such as actin filaments or microtubules, forming bundles in the presence of sufficiently high concentrations of multivalent cations, as shown in the past both experimentally and theoretically.[31–34] The valency-dependence is also reminiscent to the compaction of double-stranded DNA by multivalent cations, where the neutralization of the DNA backbone through counter-ion condensation drives the process.[35] According to the Manning-Oosawa picture,[36,37] counter-ions of valency z condense on the DNA backbone leading to an average charge neutralization $\theta = 1 - d/(zl_B)$ where d is the average distance between DNA charges (0.17 nm) and l_B is

the Bjerrum length ($l_B = e^2/(4\pi\varepsilon k_B T)$, with the e the elementary charge, ε the dielectric constant of the solvent, k_B the Boltzmann constant and T the temperature). In water at 25 °C, l_B = 0.7 nm and the neutralization only depends on z: $\theta = 1 - 0.24/z$. Therefore, adding multivalent cations to double-stranded DNA induces an entropically favourable counter-ion exchange and a progressive neutralization of DNA leading to its compaction when θ becomes too large ($\approx$ 0.89).[38] The higher the valency, the more entropically favorable the counter-ion exchange is, the more efficient DNA neutralization becomes, and the lower is the charge ratio necessary to induce DNA compaction. Notably, the same evolution was observed in the nanotube condensation diagram where transitions to higher-order structures were systematically observed at a lower ρ when z increased (**Fig. 3**).

All these results showed the importance of cation valency to drive the formation of superstructures. Knowing that our buffer contained a significant amount of Mg^{2+} (12.5 mM), we performed the same study in a buffer composed of solely monovalent cations. To get stable nanotubes, we replaced $MgCl_2$ by a high concentration of NaCl (100 mM).[11] Interestingly, we obtained the same types of superstructures by adding increasing amounts of SPM^{4+} (**Fig. S6**), including the formation of rings (**Fig. S7)** having dimensions similar to those obtained in the regular Mg^{2+}-containing buffer (**Fig 2E**). All these results showed that the multivalent counter-ions were the main driving force for the superstructure formation. Note that the frontiers for the transitions were shifted to higher charge ratios ρ when Na^+ was used (ρ = 21.4 for the nanotube-network and ρ = 89.3 for the network-bundle transition, **Fig. S6**) instead of Mg^{2+} (ρ = 7.14 and ρ = 14.3, **Fig. S3***)*, attributed to the large concentration of monovalent cations competing for counter-ion exchange and DNA neutralization.

The reversibility of DNA condensation led us to explore if the nanotube superstructures could be disassembled after their formation. It is known that adding an excess of monovalent cations on condensed DNA can compete with the DNA neutralization by multivalent counter-ions leading to DNA decompaction.[15] Following this principle, nanotubes were first assembled into networks by introducing [SPM^{4+}] = 0.4 mM prior to adding NaCl (100 mM) to the solution. Notably, right after Na^+ addition, nanotubes were observed freely fluctuating in solution in a state comparable to that before spermine introduction (**Fig. 4**, **Movie S2**). To achieve further control with an external stimulus without having to change the chemical composition of the medium, we implemented AzoTAB, a photosensitive DNA condensing agent.[39–42] AzoTAB is a cationic amphiphilic molecule[43–46] neutralizing DNA in a photodependent manner,[42,47] the *trans* isomer inducing DNA condensation at a lower concentration than the *cis* isomer. We used an AzoTAB solution kept in the dark (-UV, *trans*-rich state) or irradiated at 365 nm for 1 min (+UV, *cis*-rich state). Starting from individual nanotubes obtained by thermal annealing in TAMg buffer, we added different amounts of AzoTAB, without or with UV, and analyzed the resulting assemblies (**Fig. S8**). Regardless of irradiation conditions, nanotubes at a low concentration of AzoTAB (0.1 mM) were freely fluctuating in solution and appeared similar to nanotubes without

AzoTAB (**Figs. S8, 1B** *left*, and **Movie S1**). Without UV, increasing AzoTAB concentration to 0.5 and 1 mM led to the formation of clustered nanotube assemblies presenting some similarities with the networks obtained with multivalent cations. Notably, with UV, nanotubes remained individual at [AzoTAB] = 0. 5 mM and coexisted with a small fraction of restricted networks at [AzoTAB] = 1 mM (**Fig. S8**). Like for DNA condensation,[39–42] AzoTAB was thus found to induce nanotube association into superstructures at a higher concentration when a short UV irradiation was applied. As a consequence, we could identify an AzoTAB concentration (0.5 mM) where the system organized into individual nanotubes (+UV) or superstructures (-UV) in a photodependent manner (**Movie S3**). This creates ground for dynamic photoactuation of nanotube higher-order organization and superstructure formation.

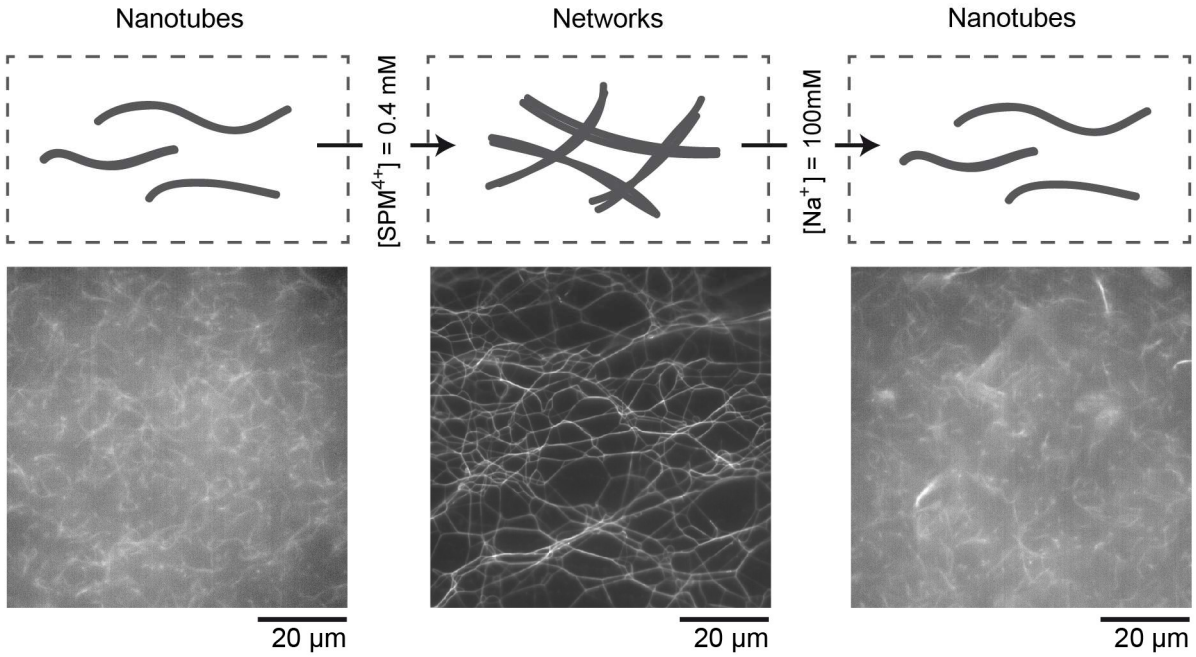

Figure 4. Reversible formation/disassembly of nanotube networks. *Schemes (top) and epifluorescence microscopy images of individual nanotubes (left), forming vast interconnected networks upon addition of 0.4 mM spermine (middle), which can be disassembled upon further addition of 100 mM NaCl (right). Each DNA strand concentration is 500 nM in TAMg buffer.*

Conclusion

We have shown that self-assembled DNA nanotubes of micrometric length condense into superstructures upon addition of sufficient amounts of multivalent cations, such as Mg^{2+}, the triamine spermidine and the tetraamine spermine. We demonstrated the strong analogy with the phenomenology of DNA condensation, through i) the crucial role of counter-ion valency (the higher the valency, the lower the charge ratio indeed to induce a transition) and ii) the formation of rings the size of the order of the nanotube persistence length resembling the toroids formed by DNA condensation and with similar

internal DNA organization. In term of the structures obtained, the system also recapitulated some of the known features obtained with other semi-flexible or rigid polyelectrolytes such as actin filaments and microtubules, with the formation of networks and bundles, thus reinforcing knowledge of the electrostatic assembly of polyelectrolytes as well as opening perspectives for building cytoskeleton-inspired materials. Mainly driven by electrostatics, the assembly principles explored here provide a ubiquitous basis for the formation of superstructures independent of their detailed chemistry. It is therefore not only a means of building higher-order superstructures combining nanoscale DNA programmability with extended dimensions, but also a strategy for organizing bricks other than DNA. The superstructure disassembly by monovalent salt addition and the photocontrol enabled in the presence of photosensitive DNA condensing agents highlight some useful principles for reconfigurable DNA assembly and constitutes ground for the elaboration of highly dynamic, multi-scale DNA-based smart materials.

Acknowledgements

This project has received funding from the European Research council ERC under the European Unions "HORIZON EUROPE Research and Innovation Programme (Grant Agreement No 101096956)" (D.B.), the Institut Universitaire de France IUF (D.B.) and the Fondation pour la Recherche Médicale FRM No ARF202209015925 (L.B.). We acknowledge the Cell and Tissue Imaging core facility (PICT IBiSA), Institut Curie, member of the French National Research Infrastructure France-BioImaging (ANR10-INBS-04). We thank David Smith (Fraunhofer Institute for Cell Therapy and Immunology) and Elisa Franco (University of California at Los Angeles) for insightful discussions.

References

(1) Seeman, N. C.; Sleiman, H. F. DNA Nanotechnology. *Nat Rev Mater* **2018**, *3* (1), 17068. https://doi.org/10.1038/natrevmats.2017.68.

(2) Rothemund, P. W. K. Folding DNA to Create Nanoscale Shapes and Patterns. *Nature* **2006**, *440* (7082), 297–302. https://doi.org/10.1038/nature04586.

(3) Wei, B.; Yin, P.; Dai, M. Complex Shapes Self-Assembled from Single-Stranded DNA Tiles. *Nature* **2013**, *485* (7400), 623–626. https://doi.org/10.1038/nature11075.

(4) Douglas, S. M.; Dietz, H.; Liedl, T.; Högberg, B.; Graf, F.; Shih, W. M. Self-Assembly of DNA into Nanoscale Three-Dimensional Shapes. *Nature* **2009**, *459* (7245), 414–418. https://doi.org/10.1038/nature08016.

(5) Ke, Y.; Ong, L. L.; Shih, W. M.; Yin, P. Three-Dimensional Structures Self-Assembled from DNA Bricks. *Science (1979)* **2012**, *338* (6111), 1177–1183. https://doi.org/10.1126/science.1227268.

(6) Ong, L. L.; Hanikel, N.; Yaghi, O. K.; Grun, C.; Strauss, M. T.; Bron, P.; Lai-Kee-Him, J.; Schueder, F.; Wang, B.; Wang, P.; Kishi, J. Y.; Myhrvold, C.; Zhu, A.; Jungmann, R.; Bellot, G.; Ke, Y.; Yin, P. Programmable Self-Assembly of Three-Dimensional Nanostructures from 10,000 Unique Components. *Nature* **2017**, *552* (7683), 72–77. https://doi.org/10.1038/nature24648.

(7) Hong, F.; Zhang, F.; Liu, Y.; Yan, H. DNA Origami: Scaffolds for Creating Higher Order Structures. *Chem Rev* **2017**, *117* (20), 12584–12640. https://doi.org/10.1021/acs.chemrev.6b00825.

(8) Knappe, G. A.; Wamhoff, E.-C.; Bathe, M. Functionalizing DNA Origami to Investigate and Interact with Biological Systems. *Nat Rev Mater* **2023**, *8* (2), 123–138. https://doi.org/10.1038/s41578-022-00517-x.

(9) Tikhomirov, G.; Petersen, P.; Qian, L. Fractal Assembly of Micrometre-Scale DNA Origami Arrays with Arbitrary Patterns. *Nature* **2017**, *552* (7683), 67–71. https://doi.org/10.1038/nature24655.

(10) Wagenbauer, K. F.; Sigl, C.; Dietz, H. Gigadalton-Scale Shape-Programmable DNA Assemblies. *Nature* **2017**, *552* (7683), 78–83. https://doi.org/10.1038/nature24651.

(11) Rossi-Gendron, C.; El Fakih, F.; Bourdon, L.; Nakazawa, K.; Finkel, J.; Triomphe, N.; Chocron, L.; Endo, M.; Sugiyama, H.; Bellot, G.; Morel, M.; Rudiuk, S.; Baigl, D. Isothermal Self-Assembly of Multicomponent and Evolutive DNA Nanostructures. *Nat Nanotechnol* **2023**, *18* (11), 1311–1318. https://doi.org/10.1038/s41565-023-01468-2.

(12) Lee Tin Wah, J.; David, C.; Rudiuk, S.; Baigl, D.; Estevez-Torres, A. Observing and Controlling the Folding Pathway of DNA Origami at the Nanoscale. *ACS Nano* **2016**, *10* (2), 1978–1987. https://doi.org/10.1021/acsnano.5b05972.

(13) Gosule, L. C.; Schellman, J. A. Compact Form of DNA Induced by Spermidine. *Nature* **1976**, *259* (5541), 333–335. https://doi.org/10.1038/259333a0.

(14) Wilson, R. W.; Bloomfield, V. A. Counterion-Induced Condensation of Deoxyribonucleic Acid. A Light-Scattering Study. *Biochemistry* **1979**, *18* (11), 2192–2196. https://doi.org/10.1021/bi00578a009.

(15) Estévez-Torres, A.; Baigl, D. DNA Compaction: Fundamentals and Applications. *Soft Matter* **2011**, *7* (15), 6746–6756. https://doi.org/10.1039/c1sm05373f.

(16) Kielar, C.; Ramakrishnan, S.; Fricke, S.; Grundmeier, G.; Keller, A. Dynamics of DNA Origami Lattice Formation at Solid-Liquid Interfaces. *ACS Appl Mater Interfaces* **2018**, *10* (51), 44844–44853. https://doi.org/10.1021/acsami.8b16047.

(17) Xin, Y.; Martinez Rivadeneira, S.; Grundmeier, G.; Castro, M.; Keller, A. Self-Assembly of Highly Ordered DNA Origami Lattices at Solid-Liquid Interfaces by Controlling Cation Binding and Exchange. *Nano Res* **2020**, *13* (11), 3142–3150. https://doi.org/10.1007/s12274-020-2985-4.

(18) Woo, S.; Rothemund, P. W. K. Self-Assembly of Two-Dimensional DNA Origami Lattices Using Cation-Controlled Surface Diffusion. *Nat Commun* **2014**, *5*, 4889. https://doi.org/10.1038/ncomms5889.

(19) Nakazawa, K.; El Fakih, F.; Jallet, V.; Rossi-Gendron, C.; Mariconti, M.; Chocron, L.; Hishida, M.; Saito, K.; Morel, M.; Rudiuk, S.; Baigl, D. Reversible Supra-Folding of User-Programmed

Functional DNA Nanostructures on Fuzzy Cationic Substrates. *Angewandte Chemie International Edition* **2021**, *60* (28), 15214–15219. https://doi.org/10.1002/anie.202101909.

(20) Mikkilä, J.; Eskelinen, A. P.; Niemelä, E. H.; Linko, V.; Frilander, M. J.; Törmä, P.; Kostiainen, M. A. Virus-Encapsulated DNA Origami Nanostructures for Cellular Delivery. *Nano Lett* **2014**, *14* (4), 2196–2200. https://doi.org/10.1021/nl500677j.

(21) Julin, S.; Korpi, A.; Nonappa; Shen, B.; Liljeström, V.; Ikkala, O.; Keller, A.; Linko, V.; Kostiainen, M. A. DNA Origami Directed 3D Nanoparticle Superlattice: Via Electrostatic Assembly. *Nanoscale* **2019**, *11* (10), 4546–4551. https://doi.org/10.1039/c8nr09844a.

(22) Rothemund, P. W. K.; Ekani-Nkodo, A.; Papadakis, N.; Kumar, A.; Fygenson, D. K.; Winfree, E. Design and Characterization of Programmable DNA Nanotubes. *J Am Chem Soc* **2004**, *126* (50), 16344–16352. https://doi.org/10.1021/ja044319l.

(23) Green, L. N.; Subramanian, H. K. K.; Mardanlou, V.; Kim, J.; Hariadi, R. F.; Franco, E. Autonomous Dynamic Control of DNA Nanostructure Self-Assembly. *Nat Chem* **2019**, *11* (6), 510–520. https://doi.org/10.1038/s41557-019-0251-8.

(24) Agarwal, S.; Klocke, M. A.; Pungchai, P. E.; Franco, E. Dynamic Self-Assembly of Compartmentalized DNA Nanotubes. *Nat Commun* **2021**, *12* (1), 3557. https://doi.org/10.1038/s41467-021-23850-1.

(25) Glaser, M.; Schnauß, J.; Tschirner, T.; Schmidt, B. U. S.; Moebius-Winkler, M.; Käs, J. A.; Smith, D. M. Self-Assembly of Hierarchically Ordered Structures in DNA Nanotube Systems. *New J Phys* **2016**, *18* (5), 055001. https://doi.org/10.1088/1367-2630/18/5/055001.

(26) Burns, J. R. Introducing Bacteria and Synthetic Biomolecules along Engineered DNA Fibers. *Small* **2021**, *17* (25). https://doi.org/10.1002/smll.202100136.

(27) Jahnke, K.; Huth, V.; Mersdorf, U.; Liu, N.; Göpfrich, K. Bottom-Up Assembly of Synthetic Cells with a DNA Cytoskeleton. *ACS Nano* **2022**, *16* (5), 7233–7241. https://doi.org/10.1021/acsnano.1c10703.

(28) Arulkumaran, N.; Singer, M.; Howorka, S.; Burns, J. R. Creating Complex Protocells and Prototissues Using Simple DNA Building Blocks. *Nat Commun* **2023**, *14* (1), 1314. https://doi.org/10.1038/s41467-023-36875-5.

(29) Illig, M.; Jahnke, K.; Weise, L. P.; Scheffold, M.; Mersdorf, U.; Drechsler, H.; Zhang, Y.; Diez, S.; Kierfeld, J.; Göpfrich, K. Triggered Contraction of Self-Assembled Micron-Scale DNA Nanotube Rings. *Nat Commun* **2024**, *15* (1), 2307. https://doi.org/10.1038/s41467-024-46339-z.

(30) Hud, N. V.; Downing, K. H. Cryoelectron Microscopy of λ Phage DNA Condensates in Vitreous Ice: The Fine Structure of DNA Toroids. *Proceedings of the National Academy of Sciences* **2001**, *98* (26), 14925–14930. https://doi.org/10.1073/pnas.261560398.

(31) Yu, X.; Carlsson, A. E. Multiscale Study of Counterion-Induced Attraction and Bundle Formation of F-Actin Using an Ising-like Mean-Field Model. *Biophys J* **2003**, *85* (6), 3532–3543. https://doi.org/https://doi.org/10.1016/S0006-3495(03)74773-0.

(32) Needleman, D. J.; Ojeda-Lopez, M. A.; Raviv, U.; Miller, H. P.; Wilson, L.; Safinya, C. R. Higher-Order Assembly of Microtubules by Counterions: From Hexagonal Bundles to Living Necklaces. *Proceedings of the National Academy of Sciences* **2004**, *101* (46), 16099–16103. https://doi.org/10.1073/pnas.0406076101.

(33) Huber, F.; Strehle, D.; Käs, J. Counterion-Induced Formation of Regular Actin Bundle Networks. *Soft Matter* **2012**, *8* (4), 931–936. https://doi.org/10.1039/c1sm06019h.

(34) Huber, F.; Strehle, D.; Schnauß, J.; Kas, J. Formation of Regularly Spaced Networks as a General Feature of Actin Bundle Condensation by Entropic Forces. *New J Phys* **2015**, *17*. https://doi.org/10.1088/1367-2630/17/4/043029.

(35) Bloomfield, V. A. DNA Condensation by Multivalent Cations. *Biopolymers* **1997**, *44* (3), 269–282. https://doi.org/https://doi.org/10.1002/(SICI)1097-0282(1997)44:3<269::AID-BIP6>3.0.CO;2-T.

(36) Manning, G. S. Limiting Laws and Counterion Condensation in Polyelectrolyte Solutions I. Colligative Properties. *J Chem Phys* **1969**, *51* (3), 924–933. https://doi.org/10.1063/1.1672157.

(37) F. Oosawa. *Polyelectrolytes*; Marcel Dekker: New-York, 1971.

(38) Baigl, D.; Yoshikawa, K. Dielectric Control of Counterion-Induced Single-Chain Folding Transition of DNA. *Biophys J* **2005**, *88* (5), 3486–3493. https://doi.org/10.1529/biophysj.105.059493.

(39) Le Ny, A. L. M.; Lee, C. T. Photoreversible DNA Condensation Using Light-Responsive Surfactants. *J Am Chem Soc* **2006**, *128* (19), 6400–6408. https://doi.org/10.1021/ja0576738.

(40) Sollogoub, M.; Guieu, S.; Geoffroy, M.; Yamada, A.; Estévez-Torres, A.; Yoshikawa, K.; Baigl, D. Photocontrol of Single-Chain DNA Conformation in Cell-Mimicking Microcompartments. *ChemBioChem* **2008**, *9*, 1201–1206. https://doi.org/10.1002/cbic.200800072.

(41) Estévez-Torres, A.; Crozatier, C.; Diguet, A.; Hara, T.; Saito, H.; Yoshikawa, K.; Baigl, D. Sequence-Independent and Reversible Photocontrol of Transcription/Expression Systems Using a Photosensitive Nucleic Acid Binder. *Proceedings of the National Academy of Sciences* **2009**, *106* (30), 12219–12223. https://doi.org/10.1073/pnas.0904382106.

(42) Diguet, A.; Mani, N. K.; Geoffroy, M.; Sollogoub, M.; Baigl, D. Photosensitive Surfactants with Various Hydrophobic Tail Lengths for the Photocontrol of Genomic DNA Conformation with Improved Efficiency. *Chemistry - A European Journal* **2010**, *16*, 11890–11896. https://doi.org/10.1002/chem.201001579.

(43) Diguet, A.; Guillermic, R.; Magome, N.; Saint-Jalmes, A.; Chen, Y.; Yoshikawa, K.; Baigl, D. Photomanipulation of a Droplet by the Chromocapillary Effect. *Angewandte Chemie International Edition* **2009**, *48* (49), 9281–9284. https://doi.org/10.1002/anie.200904868.

(44) Diguet, A.; Yanagisawa, M.; Liu, Y. J.; Brun, E.; Abadie, S.; Rudiuk, S.; Baigl, D. UV-Induced Bursting of Cell-Sized Multicomponent Lipid Vesicles in a Photosensitive Surfactant Solution. *J Am Chem Soc* **2012**, *134*, 4898–4904. https://doi.org/10.1021/ja211664f.

(45) Kavokine, N.; Anyfantakis, M.; Morel, M.; Rudiuk, S.; Bickel, T.; Baigl, D. Light-Driven Transport of a Liquid Marble with and against Surface Flows. *Angewandte Chemie International Edition* **2016**, *55* (37), 11183–11187. https://doi.org/10.1002/anie.201603639.

(46) Vialetto, J.; Anyfantakis, M.; Rudiuk, S.; Morel, M.; Baigl, D. Photoswitchable Dissipative Two-Dimensional Colloidal Crystals. *Angewandte Chemie International Edition* **2019**, *58* (27), 9145–9149. https://doi.org/10.1002/anie.201904093.

(47) Venancio-Marques, A.; Bergen, A.; Rossi-Gendron, C.; Rudiuk, S.; Baigl, D. Photosensitive Polyamines for High-Performance Photocontrol of DNA Higher-Order Structure. *ACS Nano* **2014**, *8* (4), 3654–3663. https://doi.org/10.1021/nn500266b.